

Crystal Structure of Pyridoxamine-Pyruvate Aminotransferase from *Mesorhizobium loti* MAFF303099*

Received for publication, September 27, 2007, and in revised form, October 31, 2007 Published, JBC Papers in Press, November 6, 2007, DOI 10.1074/jbc.M708061200

Yu Yoshikane[‡], Nana Yokochi[‡], Masayuki Yamasaki[§], Kimihiko Mizutani[§], Kouhei Ohnishi[¶], Bunzo Mikami[§], Hideyuki Hayashi^{||}, and Toshiharu Yagi^{‡,1}

From the [‡]Department of Bioresources Science, Faculty of Agriculture, Kochi University, Monobe-Otsu 200, Nankoku, Kochi 783-8502, Japan, the [§]Division of Food Science and Biotechnology, Graduate School of Agriculture, Kyoto University, Gokasho, Uji, Kyoto 611-0011, Japan, the [¶]Research Institute of Molecular Genetics, Kochi University, Monobe-Otsu 200, Nankoku, Kochi 783-8502, Japan, and the ^{||}Department of Biochemistry, Osaka Medical College, 2-7 Daigakumachi, Takatsuki, Osaka 569-8686, Japan

Pyridoxamine-pyruvate aminotransferase (PPAT; EC 2.6.1.30) is a pyridoxal 5'-phosphate-independent aminotransferase and catalyzes reversible transamination between pyridoxamine and pyruvate to form pyridoxal and L-alanine. The crystal structure of PPAT from *Mesorhizobium loti* has been solved in space group $P4_32_12$ and was refined to an R factor of 15.6% ($R_{\text{free}} = 20.6\%$) at 2.0 Å resolution. In addition, the structures of PPAT in complexes with pyridoxamine, pyridoxal, and pyridoxyl-L-alanine have been refined to R factors of 15.6, 15.4, and 14.5% ($R_{\text{free}} = 18.6, 18.1, \text{ and } 18.4\%$) at 1.7, 1.7, and 2.0 Å resolution, respectively. PPAT is a homotetramer and each subunit is composed of a large N-terminal domain, consisting of seven β -sheets and eight α -helices, and a smaller C-terminal domain, consisting of three β -sheets and four α -helices. The substrate pyridoxal is bound through an aldimine linkage to Lys-197 in the active site. The α -carboxylate group of the substrate amino/keto acid is hydrogen-bonded to Arg-336 and Arg-345. The structures revealed that the bulky side chain of Glu-68 interfered with the binding of the phosphate moiety of pyridoxal 5'-phosphate and made PPAT specific to pyridoxal. The reaction mechanism of the enzyme is discussed based on the structures and kinetics results.

Pyridoxamine-pyruvate aminotransferase (PPAT, EC 2.6.1.30)² is a pyridoxal 5'-phosphate (PLP)-independent aminotransferase that catalyzes the transfer of an amino group between pyridoxamine (PM) and pyruvate in the forward reaction and between pyridoxal (PL) and L-alanine in the reverse reaction. PPAT is involved in a degradation pathway for PM, one of six

natural vitamin B₆ compounds (1). It has been purified from *Pseudomonas* sp. and characterized (2). Many biochemical studies have been performed on it (3–12), because its reaction serves as a model for a half-reaction in the overall transamination reaction catalyzed by general PLP-dependent aminotransferases. Recently, we first identified the gene encoding PPAT in a nitrogen-fixing symbiotic bacterium, *Mesorhizobium loti* MAFF303099, characterized with the recombinant PPAT overexpressed in *Escherichia coli* cells (13), and found that it belonged to the class V aminotransferases of fold type I of PLP-dependent enzymes (14), although it does not use PLP as a coenzyme.

The recombinant PPAT bound the substrate PL at Lys-197 through a Schiff base, like general aminotransferases, forming an internal aldimine between PLP and an active site lysine residue, and the Schiff base formation was partially rate-determining in the reverse reaction. Sequence alignment of PPAT with other class V aminotransferases showed that the amino acid residues that have been shown to interact with PLP, based on the crystallography of *E. coli* phosphoserine aminotransferase (15) and human alanine-glyoxylate aminotransferase (AGAT; Ref. 16), were conserved in PPAT, and it was suggested that PL is held through interaction with these amino acid residues in the active site of PPAT (13). The predicted active site structure of PPAT suggested that PLP cannot bind to the enzyme because the bulky side chain of an amino acid residue located in the phosphate-binding space in PLP-dependent aminotransferases prevents the approach of PLP to the active site of PPAT (13). One of the aims of this study was to determine the amino acid residue preventing the binding of PLP, and the extent to which PPAT can be converted to PMP-pyruvate (PLP-L-alanine) aminotransferase through mutation of a relevant residue.

A further aim of this study was to propose a reaction mechanism for PPAT based on the structures of PPAT bound to PL, PM, and pyridoxyl-L-alanine (PLA) and on the profile of aligned sequences of the class V aminotransferases and kinetic results described previously (13). To assess the contribution of Arg-336 to the substrate specificity of PPAT, we produced the PPAT R336A mutant and analyzed its kinetic properties.

EXPERIMENTAL PROCEDURES

Overexpression, Purification, and Enzyme and Protein Assays—PPAT from *M. loti* MAFF303099 was overexpressed in *E. coli* cells and purified as described previously (13). The PPAT activ-

* This work was supported in part by a Grant-in-Aid for a Research Fellowship from the Japan Society for the Promotion of Science for Young Scientists. The costs of publication of this article were defrayed in part by the payment of page charges. This article must therefore be hereby marked "advertisement" in accordance with 18 U.S.C. Section 1734 solely to indicate this fact.

The atomic coordinates and structure factors (code 2Z9U, 2Z9V, 2Z9W, and 2Z9X) have been deposited in the Protein Data Bank, Research Collaboratory for Structural Bioinformatics, Rutgers University, New Brunswick, NJ (<http://www.rcsb.org/>).

¹ To whom correspondence should be addressed. Tel. and Fax: 81-88-864-5191; E-mail: yagito@cc.kochi-u.ac.jp.

² The abbreviations used are: PPAT, pyridoxamine-pyruvate aminotransferase; PM, pyridoxamine; PL, pyridoxal; PLP, pyridoxal 5'-phosphate; PMP, pyridoxamine 5'-phosphate; AGAT, alanine-glyoxylate aminotransferase; RMSD, root mean square deviation; PLA, pyridoxyl-L-alanine.

TABLE 1

Data collection and refinement statistics

Crystal	PPAT	PPAT-PM	PPAT-PL	PPAT-PLA
Data collection				
X-ray source	SPring8 (BL38B1)	SPring8 (BL38B1)	SPring8 (BL38B1)	SPring8 (BL38B1)
Wavelength (Å)	1.0000	1.0000	1.0000	1.0000
Space group	$P4_32_12$	$P4_32_12$	$P4_32_12$	$P4_32_12$
$a = b, c$ (Å)	68.545, 311.635	68.628, 312.191	68.732, 311.500	68.720, 311.942
Resolution (Å) ^a	50.00–1.90 (1.97–1.90)	50.00–1.70 (1.76–1.70)	50.00–1.60 (1.66–1.60)	50.00–1.94 (2.01–1.94)
Total number of reflections	294615	474303	737616	528717
No. of unique reflections ^a	58804 (5701)	82435 (7561)	100019 (9737)	56030 (5397)
R_{merge} ^a	0.084 (0.379)	0.039 (0.113)	0.084 (0.386)	0.071 (0.270)
Redundancy ^a	5.0 (5.6)	5.8 (3.0)	7.4 (7.4)	9.4 (9.7)
Completeness ^a	97.8 (97.2)	98.4 (91.9)	99.9 (99.9)	98.6 (97.0)
Net I over average sigma (I)	10.6	24.4	9.9	13.9
Refinement statistics				
Resolution (Å) ^a	15.00–2.00 (2.05–2.00)	14.94–1.70 (1.74–1.70)	14.84–1.70 (1.74–1.70)	14.92–1.94 (1.99–1.94)
R_{work} ^a	0.156 (0.180)	0.156 (0.168)	0.154 (0.174)	0.145 (0.157)
R_{free} ^a	0.206 (0.245)	0.186 (0.223)	0.181 (0.231)	0.184 (0.222)
No. of reflections ^a	47892 (3441)	78010 (5183)	79313 (5695)	52891 (3677)
No. of reflections (R_{free}) ^a	2551 (196)	4094 (255)	4123 (294)	2827 (208)
No. of protein residues	784	784	784	784
No. of substrate/substrate analog molecules	0	2 PM	2 PL	2 PLA
No. of glycerol molecules	4	4	7	10
No. of sulfate ions	6	5	7	8
No. of chloride ions	0	0	0	2
No. of solvent molecules (water)	550	753	778	614
RMSD bond lengths (Å)	0.015	0.010	0.010	0.013
RMSD bond angles (°)	1.440	1.248	1.243	1.342
Average B overall (Å ²)	18.596	14.852	12.800	18.258
Subunit RMSD (Å)	0.39	0.37	0.35	0.34
Ramachandran analysis (% of residues)				
Most favored	93.3	93.4	93.9	93.9
Additional allowed	6.4	6.2	5.9	5.8
Generously allowed	0.3	0.3	0.2	0.3
Disallowed	0	0	0	0

^a Statistics for the highest resolution shell are given in parentheses.

ity (by the phenylhydrazine method and the spectrophotometric method) and protein concentration (from the molecular absorption coefficient) were determined as described previously (13). PMP-pyruvate aminotransferase activity was assayed by the phenylhydrazine method as follows. The reaction mixture (0.4 ml) consisted of 0.1 M borate-KOH (pH 9.0), 5 mM sodium pyruvate, 0–5 mM PMP, and the enzyme. The reaction was performed at 30 °C for 15–30 min and stopped by the addition of 66 μ l of 9 M sulfuric acid. Kinetic parameters were determined using curve-fitting software (KaleidaGraph) as described previously (13).

Site-directed Mutagenesis of PPAT—Genes encoding E68A, E68G, and R336A mutant PPATs were prepared by essentially the same method as that described previously (13). The primers used were: for E68A, 5'-TGCATGGCGCGCCGTGC-3' and 5'-GCACCGGCGCGCCATGCA-3'; for E68G, 5'-TGCATGGCGGCGCGGTGC-3' and 5'-GCACCGGCGCGCCATGCA-3'; and for R336A, 5'-CGTCGGGGGCGGGGCGAGA-3' and 5'-TCTCGCCCCCCCCGACG-3'. The underlining indicates mismatched sites. The expressed mutant enzymes were purified by essentially the same method as that used for the wild-type enzyme (13).

Crystallization, Substrate Soaking, and X-ray Data Collection—PPAT was crystallized by the sitting drop vapor diffusion method. The volume of the reservoir solution (50 mM HEPES-KOH, pH 8.0, 2 M ammonium sulfate) was 100 μ l, and the drop volume was 5 μ l, comprising 2 μ l of a protein solution (11.6 mg/ml in 10 mM HEPES-KOH, pH 8.0, 1 mM EDTA) and 3 μ l of the reservoir solution. Single crystals appeared within 1 month at 4 °C. Crystals of PM, PL, or PLA-bound forms of

PPAT were prepared by soaking crystals in the reservoir solution containing 10 mM PM, 10 mM PL, or 5 mM PLA, respectively, for 30 min at 25 °C. PLA was synthesized from PL and L-alanine as described previously (17). All of the crystals were frozen in a cold nitrogen-gas stream after short soaking in the reservoir solution containing 30% (v/v) glycerol. X-ray diffraction data sets were collected at the BL38B1 station of SPring-8 (Hyogo, Japan) at –173 °C, using an x-ray beam with a wavelength of 1.0 Å and a Rigaku R-Axis V imaging plate detector. The crystal belongs to space group $P4_32_12$ with cell dimensions of $a = b = 68.545$ and $c = 311.625$ Å. Two molecules/asymmetric unit were estimated assuming $V_{\text{sol}} = 51\%$. All of the raw data were processed and scaled using the program suite HKL2000 (18). The parameters of the crystals and data collection are listed in Table 1.

Structure Determination and Refinement—The structure of the free form of PPAT at 2.0 Å was at first determined by the molecular replacement method, using the structure of AGAT (Ref. 19; Protein Data Bank code 1VJO) as a search model with CNS (20). After rotational and translational searches and refinements with simulated annealing, the initial model was built using TURBO-FRODO (AFMB-CNRS, Marseille, France). It was then refined further with the simulated annealing, individual B factor refinement, and energy minimization protocols in the program CNS. The noncrystallographic symmetry restraint was incorporated through the refinement, and it was removed in the final refinement. The root mean square deviation (RMSD) values of two subunits in the asymmetric units are less than 0.4 Å (Table 1). Water molecules exhibiting more than 1 σ in the $2F_o - F_c$ map and more than 3 σ in the $F_o - F_c$ map were then added to

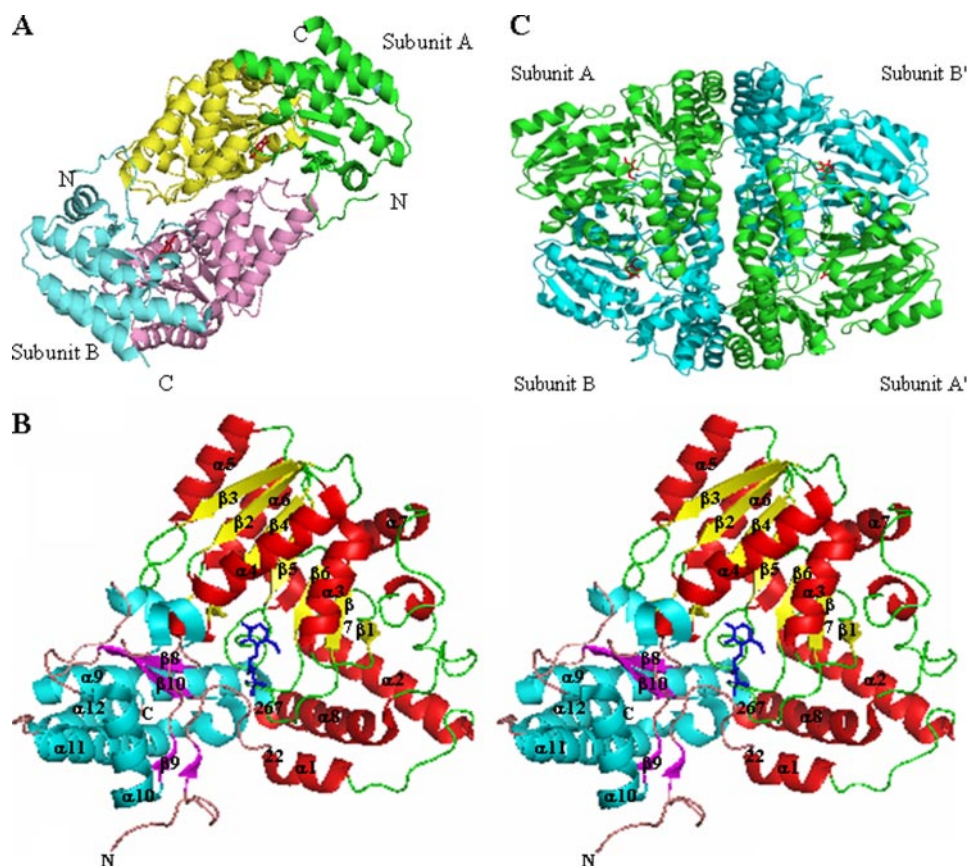


FIGURE 1. **Crystal structure of PPAT.** A, ribbon diagram of the PPAT asymmetric dimer in a complex with PL. The N-terminal domain and C-terminal domain of subunit A are shown in green and yellow, whereas those of subunit B are shown in cyan and purple, respectively. B, stereo ribbon diagram of the PPAT monomer in a complex with PL. The N-terminal domain and C-terminal domain are shown in green and yellow, respectively. Lys-197-PL is shown as a blue-colored stick model. Secondary structure elements, the N and C termini, and residues 22 and 267 are labeled. C, ribbon diagram of the PPAT tetramer in a complex with PL. The two monomers in the asymmetric unit are depicted in green and cyan, respectively. Two dimers, related through a crystallographic 2-fold axis, form a PPAT tetramer. PL is shown as a red-colored stick model. The figures were drawn with PyMOL.

the model. The structures of the PM-, PL-, and PLA-bound forms of PPAT were built using COOT (21) and refined with REFMAC5 (22) in the ccp4 suite (23). The topology and parameter files for PM and PL were obtained from the HIC-UP server (24), and those for PLA were generated using the PRODRG server (25). The stereo quality of the model was assessed using PROCHECK (26). The statistics of the data collection and the refinement are listed in Table 1.

The structural superimposition was performed using the FATCAT server (27). All of the molecular graphics figures were prepared using the program PyMOL (DeLano Scientific; pymol.sourceforge.net/). The accessible surface area was calculated with Protein-Protein Interaction Server version 1.5 (28).

Modeling of the External Aldimine of PL with L-Alanine in PPAT—For modeling of the external aldimine of PL with L-alanine in the active site of PPAT, the crystal structure of PPAT in a complex with PLA was used as the starting structure. Molecular mechanic calculations were performed using MOE (version 2006.08; Chemical Computing Group Inc., Montréal, Canada). Protons were generated on the entire structure including the water molecules. The bond between C-4' and N of the alanine moiety of PLA was changed to a double bond, the N atom

of the generated imine bond being protonated. The O-3' and N-1 of PL were unprotonated and protonated, respectively. The chloride ion was removed, and the side chain of Asn-196 was rotated around χ_1 by 135° to yield a conformation similar to that of the side chain of Asn-196 in other PPAT crystal structures (free enzyme, and the enzymes in complexes with PL and PM). Energy minimization was carried out using MMFF94s parameters with all of the atoms fixed except for those of PLA and the residue interacting with PLA, *i.e.* Lys-197, Arg-345, Tyr-95, Thr-146, Glu-68, Arg-336, and water molecules within 10 Å from PLA. Polar protons are also allowed to move.

Protein Data Bank Deposition—The coordinate and structure factors for the free enzyme, and complexes with PL, PM, and PLA have been deposited in the RCSB Protein Data Bank under accession codes 2Z9U, 2Z9V, 2Z9W, and 2Z9X, respectively.

RESULTS AND DISCUSSION

Structure Determination of PPAT—The crystal structure of PPAT from *M. loti* has been solved by means of molecular replacement and was refined to an *R* factor of 15.6% ($R_{\text{free}} = 20.6\%$) at 2.0 Å resolution. In addition,

the structures of PPAT in complexes with PM, PL, and PLA have been refined to *R* factors of 15.6, 15.4, and 14.5% ($R_{\text{free}} = 18.6, 18.1, \text{ and } 18.4\%$) at 1.7, 1.7, and 2.0 Å resolution, respectively. The final electron density maps allowed the positioning of all residues except for the first N-terminal residue (Met-1). Ramachandran plot analyses with PROCHECK (26) showed that 93–94% of the residues are in the most favored regions, and ~6% of those lie in additional allowed regions for all of the forms (Table 1).

Overall Structure of PPAT—There are two molecules (subunits)/asymmetric unit of PPAT (Fig. 1A). Each PPAT subunit consists of a large N-terminal domain (22–267), and a smaller C-terminal domain (2–21 or 268–393) (Fig. 1, A and B). The N-terminal domain has the three-layer $\alpha/\beta/\alpha$ sandwich architecture described in the CATH classification (29), and consists of eight α -helices (α_1 – α_8) and seven β -sheets (β_1 – β_7), which have a $\uparrow\beta_1 - \downarrow\beta_7 - \uparrow\beta_6 - \uparrow\beta_5 - \uparrow\beta_4 - \uparrow\beta_2 - \uparrow\beta_3$ arrangement (Fig. 1B). This domain is characteristic of PLP-dependent fold-type I aminotransferases (30). The C-terminal domain has an α/β complex architecture and consists of an N-terminal strand, four α -helices (α_9 – α_{12}), and three-stranded anti-parallel β -sheets (β_8 – β_{10}). The topology of the PPAT subunit was

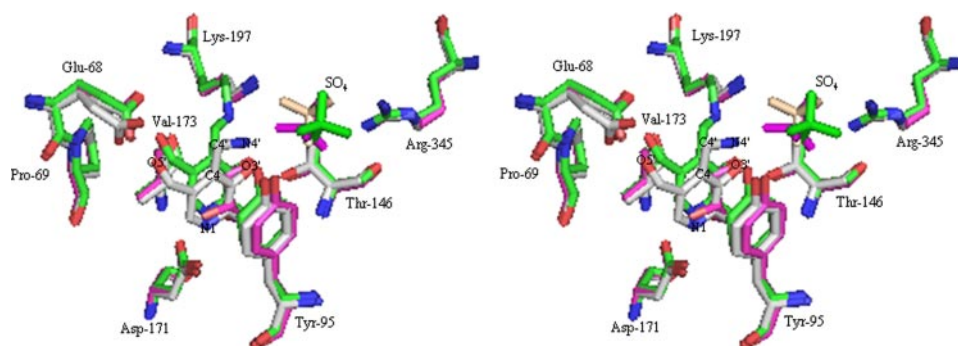


FIGURE 2. Stereo stick model of the superimposed active site structure of the free form of PPAT (magenta), and the PM-bound (white) and PL-bound (green) ones. Sulfate ions of the free form of PPAT (magenta), and the PM-bound (white) and PL-bound (green) ones are indicated. Oxygen and nitrogen atoms are shown in red and blue, respectively. The position of glycerol in the free form is hard to see, but it bound to the position corresponding to C-2', C-2, and C-3 of PM (PL). The figure was drawn with PyMOL.

basically similar to those of class V aminotransferases such as the *Saccharomyces cerevisiae* and *Nostoc* sp. AGATs (19, 31), with the exception of having an extra α -helix (α 12) at the C terminus. The mode of dimer formation by PPAT was slightly different from that in the case of AGATs because PPAT does not have the longer N-terminal strand that is found in the subunits of AGATs and stabilizes the formation of their dimers. Two dimers, related through a crystallographic 2-fold axis, form a PPAT tetramer, *i.e.* a dimer of dimers (Fig. 1C). This is in good agreement with the finding that native PPAT is a tetramer in solution when its molecular weight was determined by size exclusion chromatography (13). Two subunits (A and B) in one asymmetric unit associate with those (A' and B') in the other asymmetric one. Subunit A exhibits interface accessible surface areas of $\sim 2,000$, 200, and $1,200 \text{ \AA}^2$ as to subunits B, A', and B', respectively. Thus, subunits A and B are tightly associated through an extensive contact and exhibit 14 hydrogen bonds interactions and ~ 240 hydrophobic interactions. The dimers (AB and A'B') associate through interactions between the C-terminal domains of subunits A (B) and B' (A') and those between the C-terminal domain of subunit A (B') and the N-terminal strand (2–31 residues) of subunit B' (A). Thus, there are 20 hydrogen bonds and ~ 240 hydrophobic interactions between the dimers.

A structural homology search using MATRAS version 1.2 (32) showed that the tertiary structure of the *M. loti* PPAT subunit is similar to those of *S. cerevisiae* AGAT (Ref. 31, Protein Data Bank code 2BKW, Z score = 51.84, sequence identity 24%), *Nostoc* sp. AGAT (Ref. 19, Protein Data Bank code 1VJO, Z = 51.50, 26%), *Thermus thermophilus* aspartate aminotransferase (Ref. 33, Protein Data Bank code 1IUG, Z = 48.31, 23%), *Salmonella typhimurium* 2-aminoethylphosphonate-pyruvate aminotransferase (Ref. 34, Protein Data Bank code 1M32, Z = 42.43, 25%), and *Bacillus alcalophilus* phosphoserine aminotransferase (Ref. 35, Protein Data Bank code 1W23, Z = 34.69, 16%), all of which are class V aminotransferases of fold-type I of PLP-dependent enzymes. RMSD for PPAT, when superimposed with the *S. cerevisiae* and *Nostoc* sp. AGATs, were 1.85 \AA (for 358 C α atoms) and 1.92 \AA (for 362 C α atoms), respectively.

Active Site of PPAT and Substrate Recognition—In contrast to general aminotransferases, the native PPAT had no coenzyme forms of vitamin B₆, *i.e.* PLP or PMP (13). The residual

electron density of the free form of PPAT determined here clearly showed that it has no coenzyme. Instead, one glycerol (from the cryo-protectant solution) and one sulfate ion (from the reservoir solution) bound to the active site (Fig. 2) that is situated at the interface in the dimer (Fig. 1A). When PPAT had been incubated with PL, it bound PL through a Schiff base linkage (13). Here, it was found that PL is bound to the ϵ amino group of Lys-197 through a double bond (an external aldimine) in the active site in the PPAT-PL complex, as shown in Fig.

2. One molecule of PL bound to both subunits in the asymmetric unit. PL is stacked between Tyr-95 and Val-173 through hydrophobic interactions, and the phenol ring of Tyr-95 is situated at the *re* face of the pyridine ring of PL. The side chain of Thr-146 is hydrogen-bonded to the O-3' atom of PL, and this bond stabilizes its deprotonated state. The side chain of Thr-146 is kept in place through hydrogen bonding to O γ of Ser-174. The negative charge on the O-3' atom of PL stabilizes the protonated form of the imine nitrogen of the external aldimine because they can form an intramolecular hydrogen bond (36). Actually, the PL-Lys-197 Schiff base is protonated in a solution of pH 8.0, as determined on spectrophotometric analysis (13). The torsion angle of the C-3—C-4—C-4'—N-4' bond of the PL-lysine-197 Schiff base is 23° , and the Schiff base is roughly coplanar with the pyridine ring. The protonated Schiff base in *E. coli* aspartate aminotransferase is also nearly coplanar with the pyridine ring of PLP (36, 37). The side chain of Asp-171 forms a charged hydrogen bond with the protonated N-1 atom of PL, stabilizing the protonated N-1 to strengthen the electron-withdrawing capacity of PL (38). The side chain of Glu-68 is hydrogen-bonded to O-5' of PL. PL exhibits van der Waals' interactions with Pro-69, Cys-142, His-144, and Ser-174. The sulfate ion from the reservoir solution lies near the PL at the active site and forms charged hydrogen bonds with N η 1 and N η 2 of Arg-345. This residue corresponds to the arginine involved in the recognition of the substrate α -carboxylate in class V aminotransferases. The sulfate is also hydrogen-bonded to O η of Tyr-95 and N η 1 of Arg-336.

One molecule of PM is bound to both subunits in the asymmetric unit. In the PPAT-PM complex, PM is anchored to the same residues as those used for anchoring PL through hydrogen bonds and hydrophobic and van der Waals' interactions: Glu-68, Pro-69, Val-70, Leu-73, Tyr-95, Cys-142, His-144, Thr-146, Asp-171, Val-173, Ser-174, and the sulfate ion (Fig. 2). In contrast to for the PPAT-PL complex, PM is not covalently bound to Lys-197. Accordingly, the pyridine ring of the anchored PM tilts in the direction of Tyr-95 by $\sim 18^\circ$ around N-1. Tyr-95 itself also tilts in the same direction. N-4' of PM is hydrogen-bonded to O η of Tyr-95 and O-1 and O-4 of the sulfate ion. N-4' of PM also forms an intramolecular hydrogen-bond with O-3' of the pyridine ring. The side chain of Lys-197 is hydrogen-bonded to O of Ala-16 and O of Gly-17 and O-1 of the sulfate ion.

Structure of Pyridoxamine-Pyruvate Aminotransferase

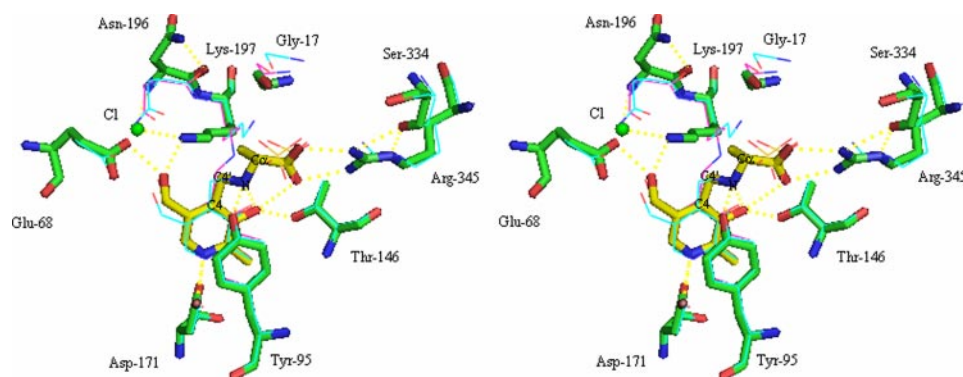


FIGURE 3. **Stereo stick model of the active site structure of PPAT in a complex with PLA.** The PLA molecule is shown in yellow, and protein residues and the chloride ion are in green. The hydrogen bonds are indicated by dotted lines. The line models are the superposed active site structures of PPAT-PM (cyan) and PPAT-PL (magenta) complexes. The figure was drawn with PyMOL.

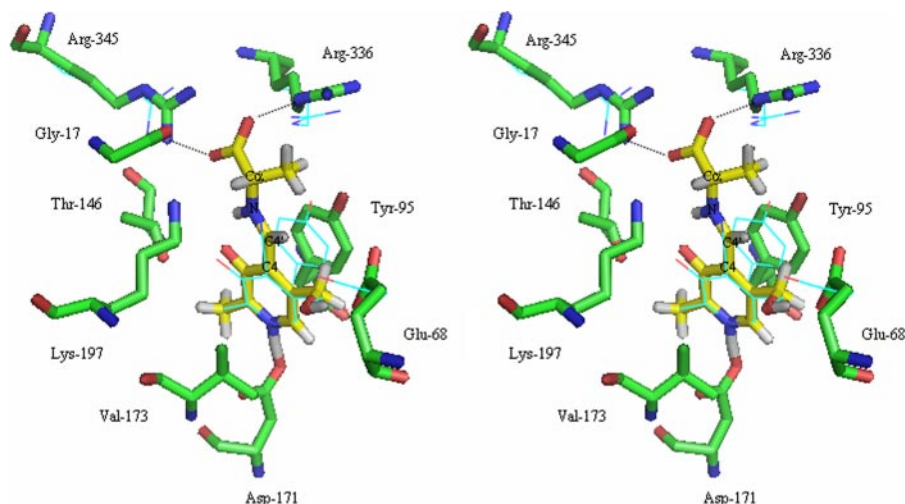


FIGURE 4. **Deduced external aldimine model.** The structure of PPAT in a complex with a Schiff base (external aldimine) between PL and L-alanine was deduced with the MOE program. The PL-alanine Schiff base is shown in yellow, and hydrogens are added to the model. The hydrogen bonds involved in the substrate α -carboxylate group binding are indicated by dotted lines. The line models are the superposed active site structure of the PPAT-PM complex (cyan). The figure was drawn with PyMOL.

The binding of PL and PM did not induce large conformational changes in the enzyme protein. The structures of the free form and the complexes could be superimposed well with C α RMSD of ~ 0.2 Å for their all C α atoms.

Binding of the Substrate Amino/Keto Acid—To identify the residues of PPAT involved in amino/keto acid binding, we determined the three-dimensional crystal structure of the enzyme in a complex with PLA, a bisubstrate analog. In the PPAT-PLA complex, the pyridoxyl moiety of PLA is anchored to the same residues as those used for anchoring PL or PM through hydrogen bonds and hydrophobic and van der Waals' interactions. The alanine moiety is recognized by Gly-17, Tyr-95, Thr-146, Pro-147, Thr-248*, Arg-336, and Arg-345 (the asterisk indicates a residue of another subunit) (Fig. 3). Arg-345 particularly forms charged hydrogen bonds with the α -carboxylate group of the alanine moiety, with distances of 2.7 and 2.8 Å. The side chain of Arg-345 is kept in place by a hydrogen-bonding network involving O of Thr-146 and O of Ser-334. Upon PLA binding, a β -turn (Ala-16–Gly-17–Pro-18–Val-19) containing the *cis* peptide bond between Gly-17 and Pro-18 on the N-terminal strand approaches the active site by 1.7 Å at the

Gly-17 C α position. The approach of this β -turn plugs the enzyme active site and thus shields PLA from the solvent environment. In the PPAT-PLA complex, the region of the twice repeated β -turns (Gly-194–Gly-204) between $\beta 6$ and $\beta 7$ in the active site also moved; the main change was movement of the side chains of Asn-196 and Lys-197. In connection with this conformational change, one chloride ion was found in the space surrounded by Asn-196, Lys-197, and Glu-68. This chloride ion forms charged hydrogen bonds with N of Asn-196 and N ϵ of Lys-197. In the free form and PPAT-PM complex, a sulfate ion forms charged hydrogen bonds with Arg-345, and the protonated side chain N ϵ of Lys-197 is attracted to the sulfate ion because of a strong negative charge. On the other hand, in the PPAT-PLA complex, this sulfate ion is absent from the model because the alanine moiety of PLA forms a hydrogen bond/salt bridge with Arg-345. The side chain of Lys-197 cannot interact with this sulfate in this model. Instead, N ϵ of Lys-197 is hydrogen-bonded to the O-5' atom of PLA because its pyridine ring is shifted up, as described below. The presence of the side chain of Lys-197 at this position displaces the side chain of Asn-196, with rotation around $\chi 1$ by 135°. As

a result, a chloride ion can be incorporated into the space previously occupied by the side chain of Asn-196.

In the PPAT-PLA complex, the distance between N ϵ of Lys-197 and C α of PLA alanine is 5.3 Å. This distance is too great if we consider that the PPAT-PLA complex represents the external aldimine complex of PPAT with alanine and that Lys-197 is the base catalyst for the prototropic shift. Moreover, there are no candidate residues that can act as the base catalyst around the PLA C α atom. This suggested that the position and conformation of PLA is not an appropriate model for the external aldimine. In fact, the absence of the double bond of C-4–C-4' and the sp³ nature of PLA alanine N allows rotation around C-4–C-4' and the formation of a hydrogen bond between PLA alanine N and the hydroxyl group of Tyr-95, both of which are not anticipated to occur in the true external aldimine between PL and alanine.

External Aldimine Model and Catalysis—To estimate the true external aldimine structure, we have calculated the energy-minimized structure of the PL-alanine Schiff base in the active site of PPAT based on the PPAT-PLA complex structure. In the external aldimine model (Fig. 4), the pyridine ring is shifted down compared with that of PLA. This is mainly caused by the

opening of the angle C-4–C-4'–N and C-4'–N–C α , because C-4' and alanine N of the external aldimine exhibit sp² hybridization, compared with those of PLA that exhibit sp³ hybridization. Accordingly, the side chain of Lys-197 does not form a hydrogen bond with O-5' of PL. The imine N atom of the external aldimine forms an intramolecular hydrogen bond with O-3' of PL, the hydrogen bond with O η of Tyr-95 being lost. As a result, the distance between the Lys-197 side chain N atom and the C α atom of the external aldimine alanine is 3.7 Å, showing that Lys-197 can be the base catalyst for the prototropic shift. Thus, the PPAT reaction can be catalyzed in the same way as those of other PLP-dependent aminotransferases by the catalytic base, Lys-197, with the catalytic assistance of Asp-171 and Thr-146.

In the external aldimine model, the alanine α -carboxylate is hydrogen-bonded to two arginine residues (Arg-345 and Arg-336). In other class V aminotransferases, the α -carboxylate is attached to an arginine residue corresponding to PPAT Arg-345 through a hydrogen bond and salt bridge (15, 39). The side chain of Arg-336 is more flexible in all forms of PPAT and lies near the alanine moiety of PLA bound to PPAT. To determine the contribution of this residue to catalysis, a mutant enzyme (R336A) in which Arg-336 was replaced with alanine was characterized. The kinetic parameters of the wild-type and R336A PPATs are shown in Table 2. The affinity for pyruvate of R336A was remarkably decreased by ~20-fold compared with that of the wild-type PPAT, whereas the affinity for PM was decreased only by ~2-fold. Thus, Arg-336 is considered to be involved in

the recognition and binding of amino/keto acid substrates in PPAT, probably by forming a hydrogen bond with the substrate α -carboxylate group.

Comparison with PLP-dependent Aminotransferases with Regard to PLP Recognition—General aminotransferases have PLP as a coenzyme. In contrast, PPAT could not bind PLP/PMP and did not catalyze the PMP-pyruvate aminotransferase reaction (13). To determine why PPAT cannot bind PLP/PMP, the active site structure of the PPAT-PL complex was superimposed on that of *Nostoc* sp. AGAT (Fig. 5). In the active site of AGAT, the phosphate group of the coenzyme is hydrogen-bonded to O of Thr-81, N of Gly-82, N and O of Thr-83, and Ne of Gln-208. Glu-68, Pro-69, Val-70, and Gln-196, respectively, occupy the corresponding positions in the active site of PPAT. Pro-69 cannot form a hydrogen bond with the phosphate group because the lone pair electrons of its main chain amide N residue are occupied by the side chain C atom. Furthermore, the two O atoms (O ϵ 1 and O ϵ 2) of Glu-68 are hydrogen-bonded to the O-5' atom of PL, the distances between them being 2.8 and 3.2 Å. Thus, there is no space for the phosphate group of PLP in the active site of PPAT because of the presence of the side chain of Glu-68. To determine the role of Glu-68 in substrate recognition, it was replaced with alanine (E68A) or glycine (E68G) with smaller side chains. As expected, the E68A and E68G PPATs showed low but detectable PMP-pyruvate aminotransferase activity (Table 2). These mutants could also bind PLP (measured spectrophotometrically; data not shown). The results showed that Glu-68 interferes with the binding of PLP/PMP phosphate and makes PPAT specific to PL/PM. On the other hand, the E68A and E68G PPATs showed the remarkably decreased activity toward PM compared with that of the wild-type PPAT (Table 2). This suggested that Glu-68 is an important residue in the catalytic reaction of PPAT.

Reaction Mechanism of PPAT—The arrangement of amino acid residues and their interactions with substrates in the active site of PPAT described above suggest that although PPAT catalyzes transamination between PL/PM and amino/keto acids, the transamination reaction proceeds via essentially the same mechanism as that in the case of general PLP-dependent aminotransferases. Lys-197 is the base catalyst for the prototropic shift. Asp-171 and Thr-146 are considered to adjust the electronic status as well as to maintain the conformation and orientation of the Schiff base. Arg-336 and Arg-345 are used for

TABLE 2
Kinetic parameters of the wild-type and mutated (R336A, E68A, and E68G) enzymes

Substrate		k_{cat} s^{-1}	K_m mM	k_{cat}/K_m $\text{s}^{-1} \text{M}^{-1}$
Wild type	PM ^a	28 \pm 0.5	0.044 \pm 0.004	640,000
	Pyruvate ^a		0.34 \pm 0.02	85,000
	PMP ^b	ND ^c	ND ^c	ND ^c
R336A	PM ^a	28 \pm 2.0	0.10 \pm 0.02	270,000
	Pyruvate ^a		6.9 \pm 0.85	4,000
E68A	PMP ^b	0.22 \pm 0.03	3.4 \pm 0.24	65
	PM ^b	0.78 \pm 0.03	1.3 \pm 0.13	590
E68G	PMP ^b	0.062 ^d	ND ^c	ND ^c
	PM ^b	0.77 \pm 0.05	2.5 \pm 0.30	310

^a The enzyme activity was determined by the spectrophotometric method.

^b The enzyme activity was determined by the phenylhydrazine method.

^c ND, not detectable.

^d The enzyme activity was determined with 5 mM PMP.

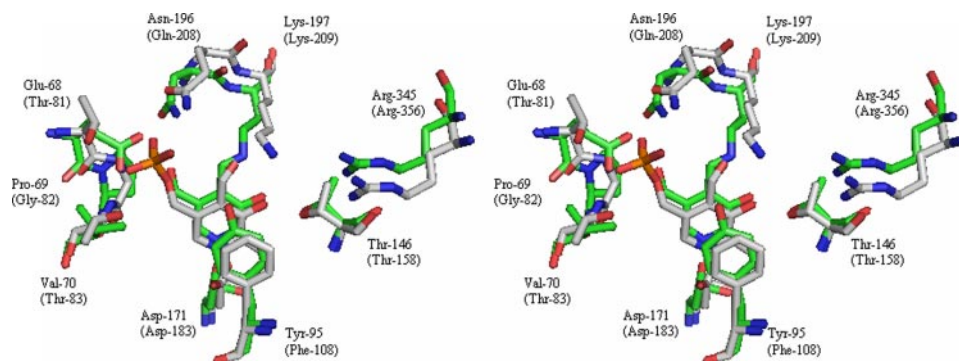
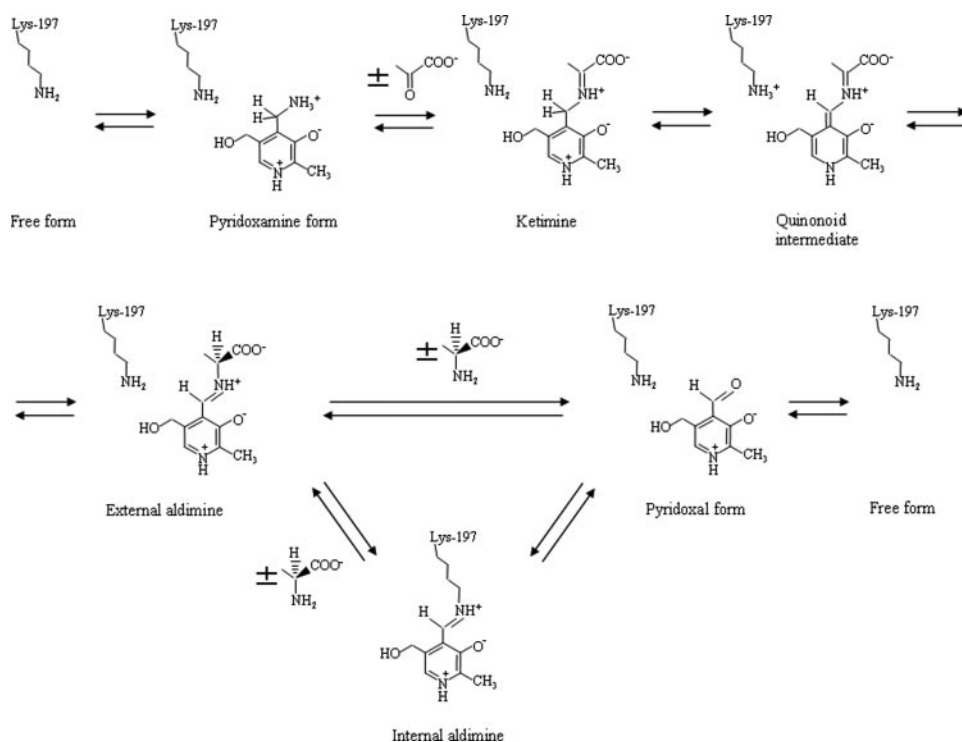


FIGURE 5. Stereo view of the superimposed active site structures of the PPAT-PL complex (green) and *Nostoc* sp. AGAT (white). Note the steric clashing of the phosphate group of PLP of AGAT with the side chain of Glu-68 of PPAT. The figure was drawn with PyMOL.

the amino/keto acid recognition. Scheme 1 shows a proposed reaction mechanism for PPAT. PPAT first binds PM and then forms a Michaelis complex with the incoming pyruvate. The ketimine is formed through nucleophilic attack of the N-4' atom of PM on the α -carbon atom of pyruvate, which is followed by the release of a water molecule. The stereospecific 1,3-prototropic shift between the ketimine and external aldimine via the quinonoid intermediate is accomplished through general base cataly-

Structure of Pyridoxamine-Pyruvate Aminotransferase



SCHEME 1. Proposed reaction mechanism of pyridoxamine-pyruvate aminotransferase.

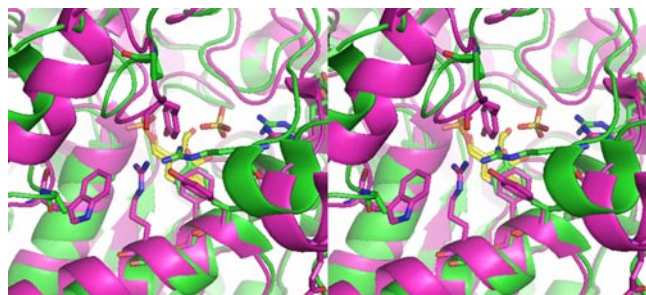


FIGURE 6. Superposition of the active sites of PPAT (green) and *Nostoc* sp. AGAT (magenta). The PL and sulfate molecules in the PPAT-PL complex and the PLP molecule in AGAT are shown as a yellow stick model. Tyr-107, Arg-111, Trp-240*, and Tyr-257* in AGAT are shown as a magenta stick model. The corresponding residues in PPAT, Val-94, Gly-98, Ala-227*, and Pro-244*, are shown as a green stick model. An asterisk indicates a residue of another subunit. Tyr-95 in PPAT (Phe-108 in AGAT) involved in the pyridine ring stacking, and Arg-345 (Arg-356) and Arg-336 involved in the amino/keto acid binding are shown as a stick model. The figure was drawn with PyMOL.

sis by Lys-197. PL and L-alanine are formed from the external aldimine and released from PPAT. There are two possible pathways for the dissociation of the external aldimine into PL and L-alanine, that is, the external aldimine may be hydrolyzed to directly form PL and L-alanine, or the external aldimine first undergoes transaldimination to form L-alanine, and a Schiff base between PL and Lys-197, and then the latter is hydrolyzed to yield the free enzyme and PL. In either case, the hydrolysis of the Schiff base is thought to be partially rate-determining, as anticipated on kinetic consideration of the K_d and K_m values of PM and PL (13). Crystallographic and spectrophotometric experiments showed that the internal Schiff base between Lys-197 and PL really exists (13). However, this does not indicate that the internal Schiff base is the necessary intermediate in the PPAT reaction. The importance of this species in

catalysis depends on the comparative formation/hydrolysis rates of the internal and external Schiff bases. This is a problem to be solved in the future.

In contrast to coenzymes PLP and PMP in general aminotransferases, substrates PL and PM should dissociate from PPAT for the next cycle of the reaction. Because PL and PM do not have a phosphate group, which is anchored in the active site through several hydrogen bonds in general aminotransferases, the strength of their interaction with PPAT should be much lower (approximately half, based on the number of hydrogen bonds), and thus they can easily dissociate from PPAT. Indeed, the *E. coli* aspartate aminotransferase Y70F mutant, in which Tyr-70 involved in the formation of a hydrogen bond with the phosphate of PLP is replaced by phenylalanine, showed lower affinity for PLP and released it more readily than the wild-type enzyme (40). Furthermore, PPAT has a side chain arrangement of residues around the active site that allows easy dissociation of substrates.

Fig. 6 shows the active site structures of PPAT and *Nostoc* sp. AGAT. The volumes of their active sites are almost the same, and their topological characters are the same. However, many residues with bulky side chains, such as Tyr-107, Arg-111, Trp-240*, and Tyr-257*, exist in the active site of the AGAT and thus shield the active site (* means a residue of another subunit). In contrast, the corresponding residues in PPAT are Val-94, Gly-98, Ala-227*, and Pro-244*, respectively. These residues have short side chains and thus would not interfere with PM and PL entering and exiting the active site of PPAT.

Here, we have determined for the first time the crystal structure of a PLP-independent aminotransferase and proposed its reaction mechanism. PM binds to the active site of PPAT and forms a tertiary complex together with pyruvate and is changed to PL with the assistance of amino acid residues located in the active site. From the evolutionary aspects, it is quite interesting to expect the presence of other types of enzymes that use PL as one substrate and racemize or decarboxylate another substrate such as an amino acid.

Acknowledgments—We thank Dr. K. Hasegawa of the Japan Synchrotron Radiation Research Institute for kind help in the data collection. X-ray data collection at BL38B1 of SPring-8 was conducted with the approval of the organizing committee of SPring-8.

REFERENCES

1. Nelson, M. J., and Snell, E. E. (1986) *J. Biol. Chem.* **261**, 15115–15120
2. Wada, H., and Snell, E. E. (1962) *J. Biol. Chem.* **237**, 133–137
3. Dempsey, W. B., and Snell, E. E. (1963) *Biochemistry* **2**, 1414–1419

4. Fujioka, M., and Snell, E. E. (1965) *J. Biol. Chem.* **240**, 3044–3049
5. Fujioka, M., and Snell, E. E. (1965) *J. Biol. Chem.* **240**, 3050–3055
6. Ayling, J. E., and Snell, E. E. (1968) *Biochemistry* **7**, 1616–1625
7. Ayling, J. E., and Snell, E. E. (1968) *Biochemistry* **7**, 1626–1636
8. Kolb, H., Cole, R. D., and Snell, E. E. (1968) *Biochemistry* **7**, 2946–2954
9. Ayling, J. E., Dunathan, H. C., and Snell, E. E. (1968) *Biochemistry* **7**, 4537–4542
10. Gilmer, P. J., McIntire, W. S., and Kirsch, J. F. (1977) *Biochemistry* **16**, 5241–5246
11. Gilmer, P. J., and Kirsch, J. F. (1977) **16**, 5246–5253
12. Hodsdon, J., Kolb, H., Snell, E. E., and Cole, R. D. (1978) *Biochem. J.* **169**, 429–432
13. Yoshikane, Y., Yokochi, N., Ohnishi, K., Hayashi, H., and Yagi, T. (2006) *Biochem. J.* **396**, 499–507
14. Grishin, N. V., Phillips, M. A., and Goldsmith, E. J. (1995) *Protein Sci.* **4**, 1291–1304
15. Hester, G., Stark, W., Moser, M., Kallen, J., Markovic-Housley, Z., and Jansonius, J. N. (1999) *J. Mol. Biol.* **286**, 829–850
16. Zhang, X., Roe, S. M., Hou, Y., Bartlam, M., Rao, Z., Pearl, L. H., and Dandpure, C. J. (2003) *J. Mol. Biol.* **331**, 643–652
17. Miles, E. W., Houck, D. R., and Floss, H. G. (1982) *J. Biol. Chem.* **257**, 14203–14210
18. Otwinowski, Z., and Minor, W. (1997) *Methods Enzymol.* **276**, 307–326
19. Han, G. W., Schwarzenbacher, R., Page, R., Jaroszewski, L., Abdubek, P., Ambing, E., Biorac, T., Canaves, J. M., Chiu, H. J., Dai, X., Deacon, A. M., DiDonato, M., Elsliger, M. A., Godzik, A., Grittini, C., Grzechnik, S. K., Hale, J., Hampton, E., Haugen, J., Hornsby, M., Klock, H. E., Koesema, E., Kreusch, A., Kuhn, P., Lesley, S. A., Levin, I., McMullan, D., McPhillips, T. M., Miller, M. D., Morse, A., Moy, K., Nigoghossian, E., Ouyang, J., Paulsen, J., Quijano, K., Reyes, R., Sims, E., Spragg, G., Stevens, R. C., van den Bedem, H., Velasquez, J., Vincent, J., von Delft, F., Wang, X., West, B., White, A., Wolf, G., Xu, Q., Zagnitko, O., Hodgson, K. O., Wooley, J., and Wilson, I. A. (2005) *Proteins* **58**, 971–975
20. Brünger, A. T., Adams, P. D., Clore, G. M., DeLano, W. L., Gros, P., Grosse-Kunstleve, R. W., Jiang, J. S., Kuszewski, J., Nilges, M., Pannu, N. S., Read, R. J., Rice, L. M., Simonson, T., and Warren, G. L. (1998) *Acta Crystallogr. Sect. D Biol. Crystallogr.* **54**, 905–921
21. Emsley, P., and Cowtan, K. (2004) *Acta Crystallogr. Sect. D Biol. Crystallogr.* **60**, 2126–2132
22. Murshudov, G. N., Vagin, A. A., and Dodson, E. J. (1997) *Acta Crystallogr. Sect. D Biol. Crystallogr.* **53**, 240–255
23. Collaborative Computational Project, Number 4 (1994) *Acta Crystallogr. Sect. D Biol. Crystallogr.* **50**, 760–763
24. Kleywegt, G. J. (2007) *Acta Crystallogr. Sect. D Biol. Crystallogr.* **63**, 94–100
25. Schuttelkopf, A. W., and van Aalten, D. M. F. (2004) *Acta Crystallogr. Sect. D Biol. Crystallogr.* **60**, 1355–1363
26. Laskowski, R. A., MacArthur, M. W., Moss, D. S., and Thornton, J. M. (1993) *J. Appl. Crystallogr.* **26**, 283–291
27. Ye, Y., and Godzik, A. (2003) *Bioinformatics* **19**, (Suppl. 2) II246–II255
28. Jones, S., and Thornton, J. M. (1996) *Proc. Natl. Acad. Sci. U. S. A.* **93**, 13–20
29. Orengo, C. A., Michie, A. D., Jones, S., Jones, D. T., Swindells, M. B., and Thornton, J. M. (1997) *Struct. Fold Des.* **5**, 1093–1108
30. Jansonius, J. N. (1998) *Curr. Opin. Struct. Biol.* **8**, 759–769
31. Meyer, P., Liger, D., Leulliot, N., Quevillon-Cheruel, S., Zhou, C. Z., Borel, F., Ferrer, J. L., Poupon, A., Janin, J., and van Tilbeurgh, H. (2005) *Biochimie (Paris)* **87**, 1041–1047
32. Kawabata, T. (2003) *Nucleic Acids Res.* **31**, 3367–3369
33. Katsura, Y., Shirouzu, M., Yamaguchi, H., Ishitani, R., Nureki, O., Kuramitsu, S., Hayashi, H., and Yokoyama, S. (2004) *Proteins* **55**, 487–492
34. Chen, C. C. H., Zhang, H., Kim, A. D., Howard, A., Sheldrick, G. M., Mariano-Dunaway, D., and Herzberg, O. (2002) *Biochemistry* **41**, 13162–13169
35. Dubnovitsky, A. P., Kapetaniou, E. G., and Papageorgiou, A. C. (2005) *Protein Sci.* **14**, 97–110
36. Hayashi, H., Mizuguchi, H., and Kagamiyama, H. (1998) *Biochemistry* **37**, 15076–15085
37. Mizuguchi, H., Hayashi, H., Okada, K., Miyahara, I., Hirotsu, K., and Kagamiyama, H. (2001) *Biochemistry* **40**, 353–360
38. Yano, T., Kuramitsu, S., Tanase, S., Morino, Y., and Kagamiyama, H. (1992) *Biochemistry* **31**, 5878–5887
39. Han, Q., Robinson, H., Gao, Y. G., Vogelaar, N., Wilson, S. R., Rizzi, M., and Li, J. (2006) *J. Biol. Chem.* **281**, 37175–37182
40. Toney, M. D., and Kirsch, J. F. (1987) *J. Biol. Chem.* **262**, 12403–12405

**Crystal Structure of Pyridoxamine-Pyruvate Aminotransferase from
Mesorhizobium loti MAFF303099**

Yu Yoshikane, Nana Yokochi, Masayuki Yamasaki, Kimihiko Mizutani, Kouhei
Ohnishi, Bunzo Mikami, Hideyuki Hayashi and Toshiharu Yagi

J. Biol. Chem. 2008, 283:1120-1127.

doi: 10.1074/jbc.M708061200 originally published online November 6, 2007

Access the most updated version of this article at doi: [10.1074/jbc.M708061200](https://doi.org/10.1074/jbc.M708061200)

Alerts:

- [When this article is cited](#)
- [When a correction for this article is posted](#)

[Click here](#) to choose from all of JBC's e-mail alerts

This article cites 39 references, 11 of which can be accessed free at
<http://www.jbc.org/content/283/2/1120.full.html#ref-list-1>